

ORIGINAL PAPER

Red quasars: estimation of SMBH spin, mass and accretion disk inclination angle

Accepted for publication in Astronomische Nachrichten

M. Yu. Piotrovich* | S. D. Buliga | T. M. Natsvlshvili

¹Central Astronomical Observatory at
Pulkovo, St.-Petersburg, Russia

Correspondence

*M. Yu. Piotrovich, Central Astronomical
Observatory at Pulkovo, St.-Petersburg,
Russia. Email: mpiotrovich@mail.ru

We estimated values of spin, mass and inclination angle for sample of 42 red quasars. Our estimations show that 2 objects: F2MS J1113+1244 and F2MS J1434+0935 with highest Eddington ratios may have geometrically thick disk. Six objects: SDSS J0036-0113, S82X 0040+0058, S82X 0118+0018, S82X 0303-0115, FBQS J1227+3214, S82X 2328-0028 may have "retrograde" rotation. Analysis of estimated spin values shows that red quasar population may contain Seyfert galaxies and NLS1.

KEYWORDS:

galaxies: nuclei, galaxies: active, accretion, accretion disks

1 | INTRODUCTION

Large ground-based optical surveys, such as the Sloan Digital Sky Survey (Lyke et al., 2020), have detected more than three-quarters of a million active galactic nuclei (AGNs). Some of these objects are sources in which we can directly observe the central object, which makes it easy to identify. However, there are darkened star systems in which the optical view of the central engine is obscured by a circumnuclear torus (Type 2 AGN) (Antonucci, 1993; Urry & Padovani, 1995) and large amounts of dust from the host galaxy. Red quasars are typically AGNs with broad emission lines, but are also covered in large amounts of dust, which reddens the spectrum and attenuates the optical emission. Studies of this extreme segment of the darkened AGN population indicate that their red color is due to the stage of AGN evolution in the black hole growth model of a major galaxy mergers, rather than to the orientation of the dust torus relative to the line of sight (Georgakakis et al., 2009; Glikman et al., 2012). According to this model, the obscuring dust is eventually dispersed by the quasar's powerful winds, revealing the quasar's luminous core. In this scenario, dust-reddened (or "red") quasars represent an early phase of supermassive black hole (SMBH)/galaxy

coevolution: the transition from a dust-covered core to a typical unobscured quasar (LaMassa et al., 2017).

Determining the spin (dimensionless angular momentum) value $a = cJ/(GM_{\text{BH}}^2)$ (where J is the angular momentum, M_{BH} is the black hole mass, and c is the speed of light) of the SMBH at the centre of an AGN is a crucial problem in modern astrophysics. The spin is thought to play a pivotal role in generating relativistic jets in AGNs; consequently, it is often the power of these relativistic jets that is used to infer the spin of the SMBH (Daly, 2011). Typically, the kinetic power of a relativistic jet is estimated by determining the magnetic field strength near the SMBH event horizon through various mechanisms, including the Blandford-Znajek mechanism (Blandford & Znajek, 1977), the Blandford-Payne mechanism (Blandford & Payne, 1982), and the Garofalo mechanism (Garofalo, Evans, & Sambruna, 2010). However in this work, we will determine spin using a different method - through radiative efficiency of accretion disk, which strongly depends on spin (Bardeen, Press, & Teukolsky, 1972; Krolik, 2007; Krolik, Hawley, & Hirose, 2007; Novikov & Thorne, 1973).

TABLE 1 Physical parameters of our objects from literature: cosmological redshift z , bolometric luminosity L_{bol} (in $\log(L_{\text{bol}}[\text{erg/s}])$), Eddington ratio l_E and SMBH mass M_{BH} (in $\log(M_{\text{BH}}/M_{\odot})$), and estimated values of inclination angle $i_{1,2,3}$ (in [deg]), mass $M_{\text{BH},1,2,3}$ and spin $a_{1,2,3}$ for 3 models: (1) Raimundo et al. (2012), (2) Trakhtenbrot (2014), (3) Du et al. (2014).

Object	$\log z$	L_{bol}	$\log l_E$	M_{BH}	i_1	$M_{\text{BH},1}$	a_1	i_2	$M_{\text{BH},2}$	a_2	i_3	$M_{\text{BH},3}$	a_3
S82X 0011+0057	0.173	46.02 ³	-0.96 ³	8.85 ³	60	8.73	0.982	45	8.91	0.968	50	8.84	0.998
S82X 0022+0020	-0.097	45.85 ³	-1.00 ²	8.75 ³	50	8.74	0.998	45	8.81	0.970	50	8.74	0.998
SDSS J0036-0113	-0.081	45.79 ⁷	-0.08 ⁷	7.78 ⁷	35	7.56	-0.506	25	7.83	-0.452	30	7.68	-0.506
S82X 0040+0058	-0.091	45.12 ³	-0.29 ⁰	7.30 ³	45	7.36	-0.354	40	7.44	-0.754	45	7.36	-0.824
S82X 0043+0052	-0.082	45.93 ³	-1.05 ³	8.84 ³	60	8.72	0.990	45	8.90	0.980	55	8.77	0.986
S82X 0100+0008	0.173	45.52 ³	-1.00 ³	8.43 ³	45	8.01	0.644	45	8.01	0.232	45	8.01	0.682
S82X 0118+0018	0.043	45.41 ³	-0.69 ⁰	7.99 ³	45	7.57	-0.824	40	7.65	-0.686	45	7.57	-0.624
S82X 0242+0005	0.394	47.24 ³	-0.49 ³	9.62 ³	50	9.45	0.998	45	9.52	0.890	50	9.45	0.990
S82X 0302-0003	0.099	46.85 ³	-0.64 ³	9.38 ³	45	9.20	0.998	45	9.20	0.828	45	9.20	0.994
S82X 0303-0115	-0.228	45.17 ³	-0.39 ³	7.44 ³	25	7.44	-0.038	25	7.44	-0.354	30	7.29	-0.624
F2M J0729+3336	-0.019	46.91 ⁴	0.10 ⁴	8.70 ⁴	45	8.74	0.882	45	8.74	-0.354	45	8.74	0.598
F2MS J0825+4716	-0.095	47.35 ²	-0.17 ²	9.10 ⁵	45	8.99	0.900	45	8.99	-0.506	45	8.99	0.608
F2M J0830+3759	-0.383	45.59 ⁶	-0.40 ⁴	8.60 ⁴	45	8.05	0.852	45	8.05	0.186	45	8.05	0.676
F2MS J0834+3506	-0.328	46.18 ²	-1.40 ²	9.50 ²	70	9.11	0.992	50	9.29	0.998	65	9.14	0.990
F2MS J0841+3604	-0.257	46.21 ⁴	-0.40 ⁴	8.50 ⁴	45	8.40	0.884	45	8.40	-0.004	45	8.40	0.668
F2MS J0911+0143	-0.220	46.19 ⁷	-0.31 ⁷	8.40 ⁷	45	8.46	0.934	45	8.46	0.254	45	8.46	0.778
F2MS J0915+2418	-0.074	47.70 ²	-0.03 ²	9.00 ⁷	45	9.06	0.804	40	9.14	-0.506	45	9.06	0.332
F2MS J1012+2825	-0.028	47.31 ⁴	-0.10 ⁴	9.30 ⁴	50	9.29	0.994	45	9.36	0.682	45	9.36	0.978
F2M J1106+4807	-0.362	46.73 ²	-0.28 ²	8.90 ²	45	8.96	0.996	45	8.96	0.618	45	8.96	0.946
F2MS J1113+1244	-0.167	47.48 ²	0.36 ²	8.50 ⁷	45	9.36	0.998	45	9.36	0.500	45	9.36	0.946
F2MS J1118-0033	-0.164	46.94 ²	0.04 ²	8.80 ²	45	8.86	0.946	45	8.86	0.026	45	8.86	0.762
F2MS J1151+5359	-0.108	46.57 ²	-0.30 ²	8.80 ²	45	8.86	0.994	45	8.86	0.618	45	8.86	0.940
SDSS J1209-0107	-0.442	46.51 ⁷	-0.52 ⁷	8.90 ⁷	50	8.89	0.994	45	8.96	0.804	45	8.96	0.986
FBQS J1227+3214	-0.863	45.55 ²	-0.10 ²	7.40 ¹	40	7.54	-0.220	30	7.76	-0.220	35	7.64	-0.180
F2MS J1227+5053	-0.116	46.35 ⁷	-0.19 ⁷	8.50 ⁷	45	8.67	0.982	45	8.67	0.524	45	8.67	0.902
F2MS J1248+0531	-0.126	46.28 ⁷	-0.20 ⁷	8.40 ⁷	45	8.46	0.906	45	8.46	0.084	45	8.46	0.710
F2MS J1307+2338	-0.561	45.51 ⁷	-0.28 ⁷	7.70 ⁷	45	7.76	0.430	45	7.76	-0.824	45	7.76	0.026
SDSS J1309+6042	-0.193	46.26 ⁷	-0.21 ⁷	8.40 ⁷	45	8.09	0.294	35	8.27	-0.180	45	8.09	-0.452
F2MS J1313+1453	-0.234	46.67 ⁷	-0.30 ⁷	8.90 ⁷	45	8.96	0.998	45	8.96	0.676	45	8.96	0.960
F2M J1324+0537	-0.688	46.72 ²	-0.12 ²	8.70 ²	45	8.76	0.950	45	8.76	0.162	45	8.76	0.788
F2MS J1434+0935	-0.114	46.59 ⁷	0.53 ⁷	8.00 ⁷	45	8.70	0.952	45	8.70	0.232	45	8.70	0.804
F2M J1507+3129	-0.005	46.93 ²	0.17 ²	8.70 ²	45	8.76	0.886	45	8.76	-0.354	45	8.76	0.608
F2M J1531+2423	0.359	48.21 ²	0.21 ²	9.90 ²	55	9.83	0.996	45	9.96	0.758	45	9.96	0.998
F2MS J1532+2415	-0.249	46.57 ²	-0.54 ²	8.80 ²	45	8.86	0.994	45	8.86	0.618	45	8.86	0.940
F2MS J1540+4923	-0.157	46.44 ⁷	-0.72 ⁷	9.10 ⁷	60	8.98	0.990	45	9.16	0.962	50	9.09	0.998
F2MS J1600+3522	-0.151	46.63 ⁷	0.29 ⁷	8.30 ⁷	45	8.36	0.524	40	8.44	-0.686	45	8.36	-0.106
F2MS J1656+3821	-0.135	46.81 ²	-0.12 ²	8.70 ⁷	45	8.76	0.928	45	8.76	-0.038	45	8.76	0.724
F2M J1715+2807	-0.281	46.55 ²	-0.48 ²	8.90 ²	50	8.89	0.992	45	8.96	0.778	45	8.96	0.982
F2MS J1720+6156	-0.138	46.41 ⁷	0.21 ⁷	8.10 ⁷	45	8.39	0.778	45	8.39	-0.564	45	8.39	0.416
F2MS J2325-1052	-0.249	46.31 ⁷	-0.21 ⁷	8.40 ⁷	45	8.72	0.994	45	8.72	0.652	45	8.72	0.942
S82X 2328-0028	-0.232	45.08 ³	-0.38 ³	7.34 ³	45	7.40	-0.824	40	7.48	-0.402	45	7.40	-0.452
F2MS J2339-0912	-0.180	46.90 ⁷	0.04 ⁷	8.80 ⁷	45	8.50	0.548	40	8.58	-0.824	45	8.50	-0.142

(0) Our calculations; (1) Glikman, LaMassa, Piconcelli, Urry, and Lacy (2017);

(2) Glikman, LaMassa, Piconcelli, Zappacosta, and Lacy (2024); (3) LaMassa et al. (2017); (4) Urrutia et al. (2012);

(5) Kim, Im, Glikman, Woo, and Urrutia (2015); (6) LaMassa et al. (2016); (7) Kim and Im (2018).

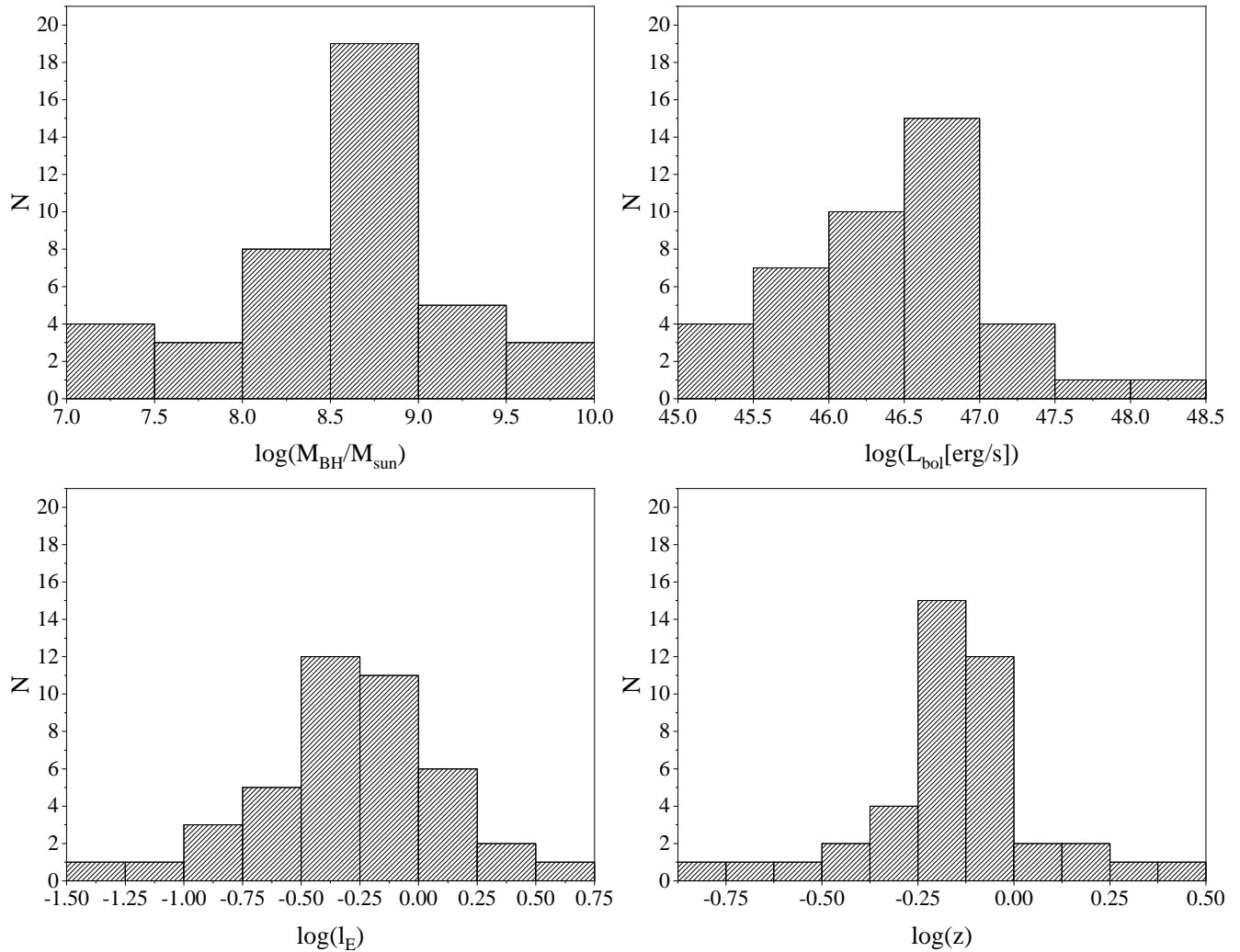


FIGURE 1 Distributions of the parameters of objects from the initial set: SMBH mass M_{BH} , bolometric luminosity L_{bol} , Eddington ratio l_E and redshift z .

2 | ANALYSIS OF THE INITIAL DATA

We selected a set of 42 red quasars with known physical parameters from literature (Glikman et al., 2017, 2024; Kim & Im, 2018; Kim et al., 2015; LaMassa et al., 2017, 2016; Urrutia et al., 2012). First 5 columns of Table 1 show: object name, redshift, bolometric luminosity, Eddington ratio and SMBH mass.

Then we carried out statistical analysis of our set. Fig. 1 shows the distributions of the parameters of our objects.

It can be seen that the SMBHs mass M_{BH} distribution is quite close to log-normal with a slight drop in the region of high masses and with a maximum in the region $8.5 < \log(M_{\text{BH}}/M_{\odot}) < 9.0$, which is slightly higher than the similar value for all AGNs, which is usually taken to be equal to ~ 8 .

The distribution of the bolometric luminosity L_{bol} is also close to log-normal with a drop in the region of high luminosities and with a maximum in the range $46.5 < \log(L_{\text{bol}}[\text{erg/s}]) < 47.0$.

The distribution of the Eddington ratio l_E appears log-normal, but with a less pronounced peak in the region $-0.50 < \log(l_E) < -0.25$. It can be noted that the luminosity of most objects is below Eddington luminosity, but there are several objects with quite high luminosity, up to ~ 3 Eddington luminosities.

The cosmological redshift z distribution looks quite typical for such objects. The increase at small z is associated with an increase in the number of objects with distance, and the decrease at large z is due to the fact that at large distances objects are much more difficult to observe.

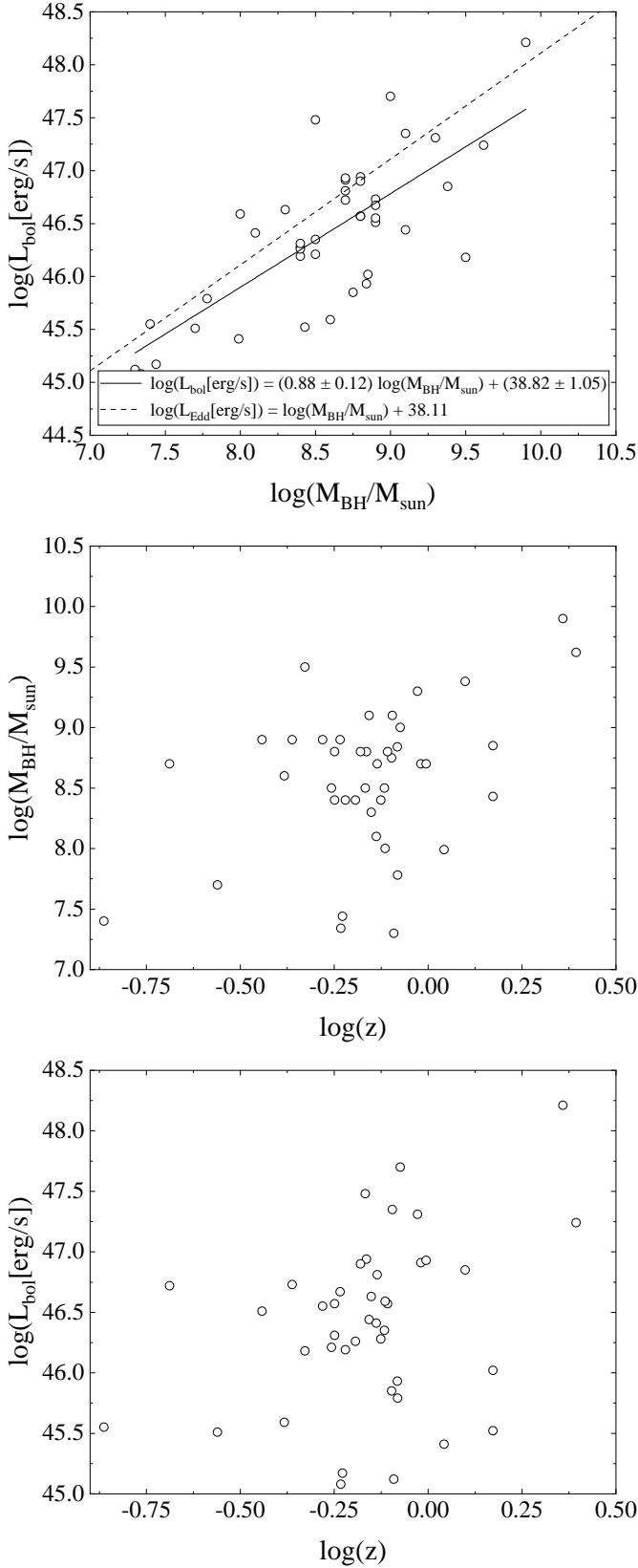


FIGURE 2 Dependencies of the physical parameters of objects from the initial set on each other.

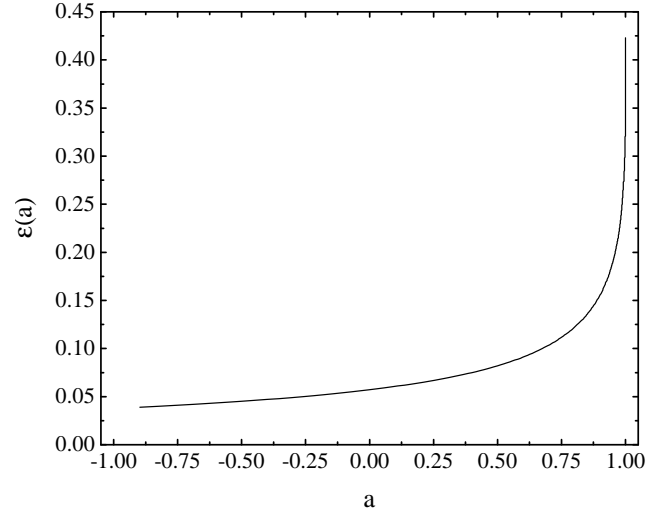


FIGURE 3 Dependence of the radiative efficiency ϵ on the spin a (see Eqs.(6,7)).

Fig. 2 shows the dependencies of the physical parameters of our objects on each other.

One can see that the bolometric luminosity clearly correlates with the SMBH mass (Spearman correlation coefficient is 0.65) and linear fitting gives us: $\log(L_{\text{bol}} [\text{erg/s}]) = (0.88 \pm 0.12) \log(M_{\text{BH}}/M_{\odot}) + (38.82 \pm 1.05)$, which is close to Eddington luminosity $\log(L_{\text{Edd}}) = \log(M_{\text{BH}}/M_{\odot}) + 38.11$. As for the dependencies of SMBHs mass and luminosity on redshift, it can be seen that there is no correlation between parameters (Spearman correlation coefficients are 0.22 and 0.25 respectively). This is expected behavior for this number of objects.

3 | METHOD FOR ESTIMATING SPIN VALUES

One approach to estimating the spin of a black hole is by determining the radiative efficiency $\epsilon(a)$ of its accretion disk. This efficiency depends on the value of the black hole's spin (Bardeen et al., 1972; Krolik, 2007; Krolik et al., 2007; Novikov & Thorne, 1973) (see Fig. 3). The radiative efficiency is defined as $\epsilon = L_{\text{bol}}/(\dot{M}c^2)$, where L_{bol} is the AGN bolometric luminosity and \dot{M} is the accretion rate. For this estimation, the value of radiative efficiency should fall within the range $0.039 < \epsilon < 0.324$, and the spin $-1.0 < a \leq 0.998$ (Thorne, 1974). A negative value of the spin corresponds to "retrograde" rotation, where the SMBH and its accretion disk rotate in opposite directions.

The radiative efficiency coefficient has been related to various AGN parameters, including the SMBH mass M_{BH} , the

angle between the line of sight and the normal to the accretion disk plane i , and the bolometric luminosity L_{bol} (Davis & Laor, 2011; Du et al., 2014; Lawther, Vestergaard, Raimundo, & Grupe, 2017; Raimundo et al., 2012; Trakhtenbrot, 2014). These relationships are based on statistical analyses of observational data and the Shakura-Sunyaev accretion disk model (Shakura & Sunyaev, 1973). The methods proposed by Davis and Laor (2011) and Raimundo et al. (2012), as well as Lawther et al. (2017), all rely on this framework. The methods by Davis and Laor (2011) and Raimundo et al. (2012) are essentially equivalent, while the approach by Lawther et al. (2017) can be considered a variation of the earlier work by Raimundo et al. (2012). Given these similarities, we have chosen to focus on three distinct models that differ from one another in meaningful ways. To facilitate comparison and analysis, we have reformulated the equations presented in the original papers to achieve greater uniformity:

1. Du et al. (2014):

$$\epsilon(a) = 0.105 \left(\frac{L_{\text{bol}}}{10^{46} \text{ erg/s}} \right) \left(\frac{L_{5100}}{10^{45} \text{ erg/s}} \right)^{-1.5} M_8 \mu^{1.5}.$$

2. Raimundo et al. (2012):

$$\epsilon(a) = 0.063 \left(\frac{L_{\text{bol}}}{10^{46} \text{ erg/s}} \right)^{0.99} \left(\frac{L_{\text{opt}}}{10^{45} \text{ erg/s}} \right)^{-1.5} M_8^{0.89} \mu^{1.5}.$$

3. Trakhtenbrot (2014):

$$\epsilon(a) = 0.073 \left(\frac{L_{\text{bol}}}{10^{46} \text{ erg/s}} \right) \left(\frac{\lambda L_\lambda}{10^{45} \text{ erg/s}} \right)^{-1.5} \left(\frac{\lambda}{5100 \text{ \AA}} \right)^{-2} M_8 \mu^{1.5}$$

$$\lambda L_\lambda = L_{\text{opt}}, \lambda = 4400 \text{ \AA}.$$

Here L_{5100} is the luminosity at 5100 \AA , $M_8 = M_{\text{BH}}/(10^8 M_\odot)$ and $\mu = \cos(i)$. For the model from Du et al. (2014), we used the Eddington ratio $l_E = L_{\text{bol}}/L_{\text{Edd}}$, where $L_{\text{Edd}} = 1.3 \times 10^{38} M_{\text{BH}}/M_\odot \text{ erg/s}$ is the Eddington luminosity.

In the literature, we were able to find L_{5100} for only 7 objects, so for the remaining objects we calculated these values using known L_{bol} and bolometric correction (Richards et al., 2006): $L_{5100} = L_{\text{bol}}/10.3$.

As for the angle i , its reliable determination from observational data is a rather complicated and not yet fully solved problem. Many authors often just assume that i equals to some average constant value for all objects. In this work, we employed the following approach: for each object, we took the average value of the angle $i = 45^\circ$; if the current numerical method did not yield a physically meaningful result, then we alternately changed the angles to smaller and larger values with a step size of 5° until achieving a meaningful outcome.

It should be noted that determined mass of SMBH actually depends on inclination angle i , since the most widely used method for determining mass uses expressions of the form (Decarli, Labita, Treves, & Falomo, 2008):

$$M_{\text{BH}} = \frac{R_{\text{BLR}} V_{\text{BLR}}^2}{G}, \quad (1)$$

where R_{BLR} is the accretion disk broad-line region (BLR) scale radius, V_{BLR} is the typical velocity of matter in BLR and G is the gravitational constant. V_{BLR} can be determined through observations, namely by measuring full width at half maximum (FWHM) of $H\beta$ spectral line:

$$V_{\text{BLR}} = f \times FWHM(H\beta). \quad (2)$$

Here f is coefficient describing the geometry of the accretion disk that, using some general assumptions (see Decarli et al. (2008)), can be expressed as:

$$f = \left(2 \sqrt{\left(\frac{H}{R} \right)^2 + \sin^2 i} \right)^{-1}, \quad (3)$$

where H/R is basically a ratio of the geometric thickness of the disk to the disk radius. In this work we assume that all objects have geometrically thin disks, so $H/R \ll 1$ and

$$f \approx \frac{1}{2 \sin i}. \quad (4)$$

One of the popular methods for determining R_{BLR} from observations is the method from Collin and Kawaguchi (2004):

$$R_{\text{BLR}} = 32.9 \times \left(\frac{L_{5100}}{10^{44} \text{ erg/s}} \right)^{0.7}. \quad (5)$$

When determining SMBH mass, it is usually assumed by default that $f = \sqrt{3}/2$ (in our case it corresponds to $i \approx 35^\circ$) (Collin & Kawaguchi, 2004; Decarli et al., 2008). Thus, when we estimated radiative efficiencies for various values of inclination angle we also for self-consistency estimated new mass values (using Eq.(1)), assuming that initial mass from the literature was obtained for $i \approx 35^\circ$.

Then the spin values were determined numerically using the method from Bardeen et al. (1972) (see Fig.3):

$$\epsilon(a) = 1 - \frac{R_{\text{ISCO}}^{3/2} - 2R_{\text{ISCO}}^{1/2} + |a|}{R_{\text{ISCO}}^{3/4} \left(R_{\text{ISCO}}^{3/2} - 3R_{\text{ISCO}}^{1/2} + 2|a| \right)^{1/2}}, \quad (6)$$

where R_{ISCO} is the radius of the innermost stable circular orbit that depends on spin:

$$\begin{aligned} R_{\text{ISCO}}(a) &= \\ &= 3 + Z_2 \pm [(3 - Z_1)(3 + Z_1 + 2Z_2)]^{1/2}, \\ Z_1 &= 1 + (1 - a^2)^{1/3} [(1 + a)^{1/3} + (1 - a)^{1/3}], \\ Z_2 &= (3a^2 + Z_1^2)^{1/2}. \end{aligned} \quad (7)$$

Here “-” is used when $a \geq 0$, and “+” when $a < 0$.

4 | RESULTS OF OUR ESTIMATIONS

We have estimated values of spin, mass and inclination angle for all 42 objects from our set using 3 models. The results are shown at Table 1 .

One can see that our mass estimations are close to literature data (considering that average error in literature data is

± 0.1 in logarithmic scale) for almost all objects except for F2MS J1113+1244 and F2MS J1434+0935, which, at the same time, have highest values of Eddington ratio $l_E = 2.29$ and $l_E = 3.35$ respectively. This may indicate that for objects with such high super-Eddington luminosity our assumption about geometrically thin disk is wrong (or that the mass of these objects is determined incorrectly). However, we note that for super-Eddington objects with $l_E < 2.0$ our assumption seems to work quite well.

For 6 objects (SDSS J0036-0113, S82X 0040+0058, S82X 0118+0018, S82X 0303-0115, FBQS J1227+3214, S82X 2328-0028) all 3 models produce a negative spin value, which may indicate the presence of "retrograde" rotation, which can be evidence of a recent merger. It should be noted that some authors generally believe that the observed properties of the majority or even all red quasars are associated with recent mergers. Of this six objects, we were able to find in the literature some additional evidences of recent merger for FBQS J1227+3214 (Glikman et al., 2024).

Fig. 4 shows distributions of estimated spin values for 3 models. It can be seen that first and, to some extent, third models demonstrate similar distributions, which are quite characteristic of AGNs with high z values (Trakhtenbrot, 2014) and Seyfert galaxies (Afanasiev, Gnedin, Piotrovich, Natsvlshvili, & Buliga, 2018; M. Piotrovich, Buliga, & Natsvlshvili, 2023; M. Y. Piotrovich, Buliga, & Natsvlshvili, 2022). Second model demonstrates a rather strange and atypical distribution which may indicate that this model is not suitable for determining spins of this type of objects.

Fig. 5 demonstrates distribution of estimated inclination angles for 3 models. Pronounced peak near 45° is associated with the calculation method we used. Our method for estimating inclination angle, of course, is not completely accurate, however it is significantly more accurate than the method that simply uses one average constant angle value for all objects.

Fig. 6 shows distributions of estimated SMBH masses for 3 models. All distributions look similar to distribution of initial masses from literature, what is the expected result.

Fig. 7 displays dependencies of the spin on the redshift for 3 models. There is no detectable correlation between parameters for all models (Spearman correlation coefficients are 0.06, 0.05 and 0.1 respectively). This is expected result due to the small number of objects.

Fig. 8 shows dependencies of the spin on the SMBH mass for 3 models. The correlation between the parameters is prominent (Spearman correlation coefficients are 0.82, 0.67 and 0.79 respectively). The linear fitting gives us:

$$\begin{aligned} a_1 &= (0.73 \pm 0.07) \log(M_{\text{BH},1}/M_\odot) - (5.56 \pm 0.64), \\ a_2 &= (0.67 \pm 0.12) \log(M_{\text{BH},2}/M_\odot) - (5.65 \pm 1.03), \\ a_3 &= (0.76 \pm 0.08) \log(M_{\text{BH},3}/M_\odot) - (6.13 \pm 0.69). \end{aligned} \quad (8)$$

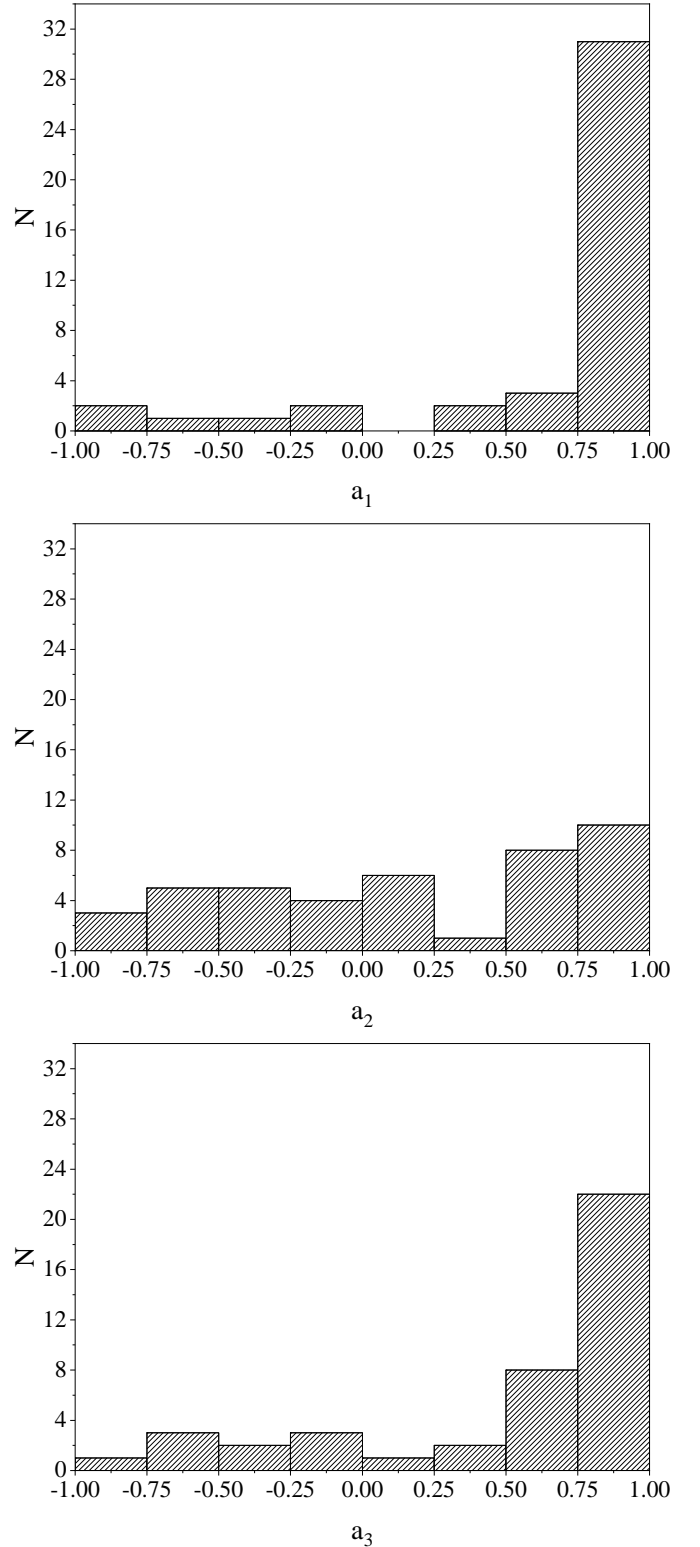


FIGURE 4 Distributions of estimated spins for 3 models.

In our previous work (M. Y. Piotrovich et al., 2022) we obtained similar ratio for Seyfert galaxies, but with a slope value of $\sim 0.3 - 0.45$. And for Narrow Line Seyfert galaxies

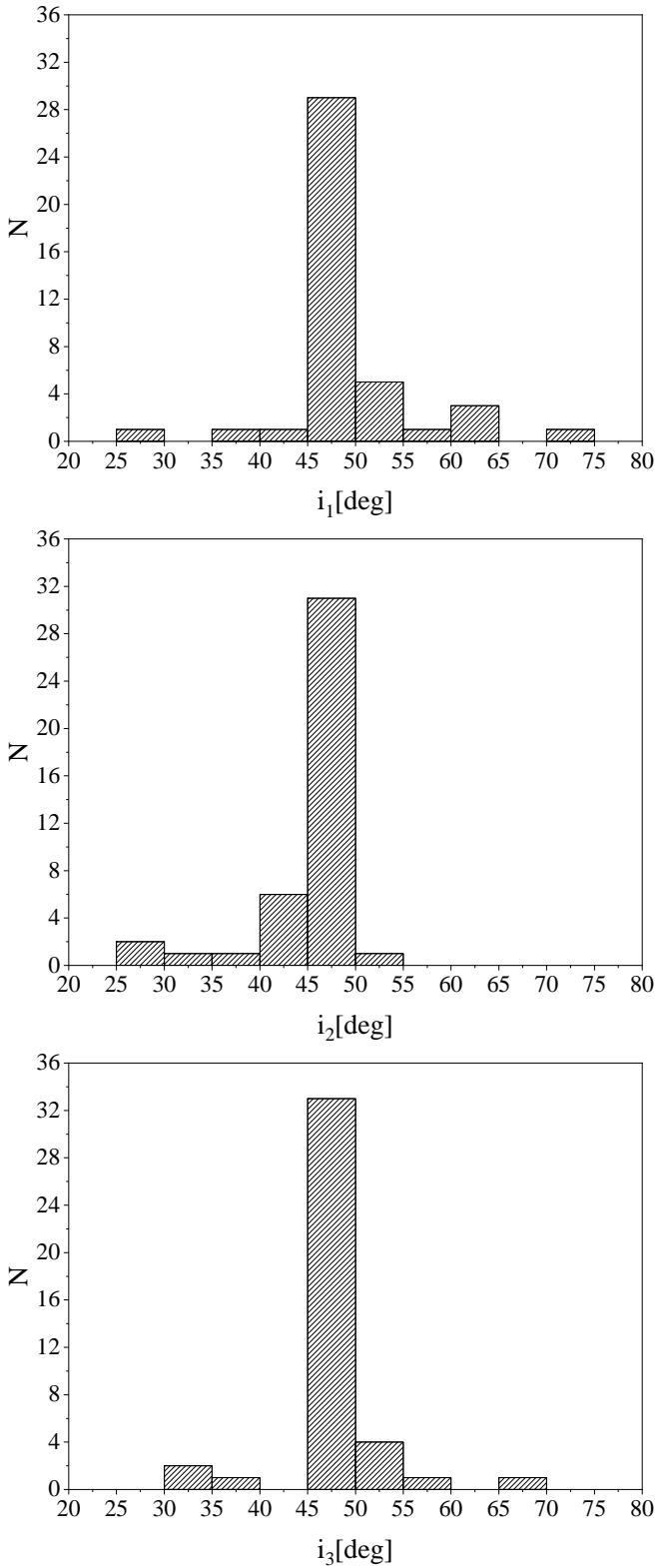


FIGURE 5 Distributions of estimated inclination angles for 3 models.

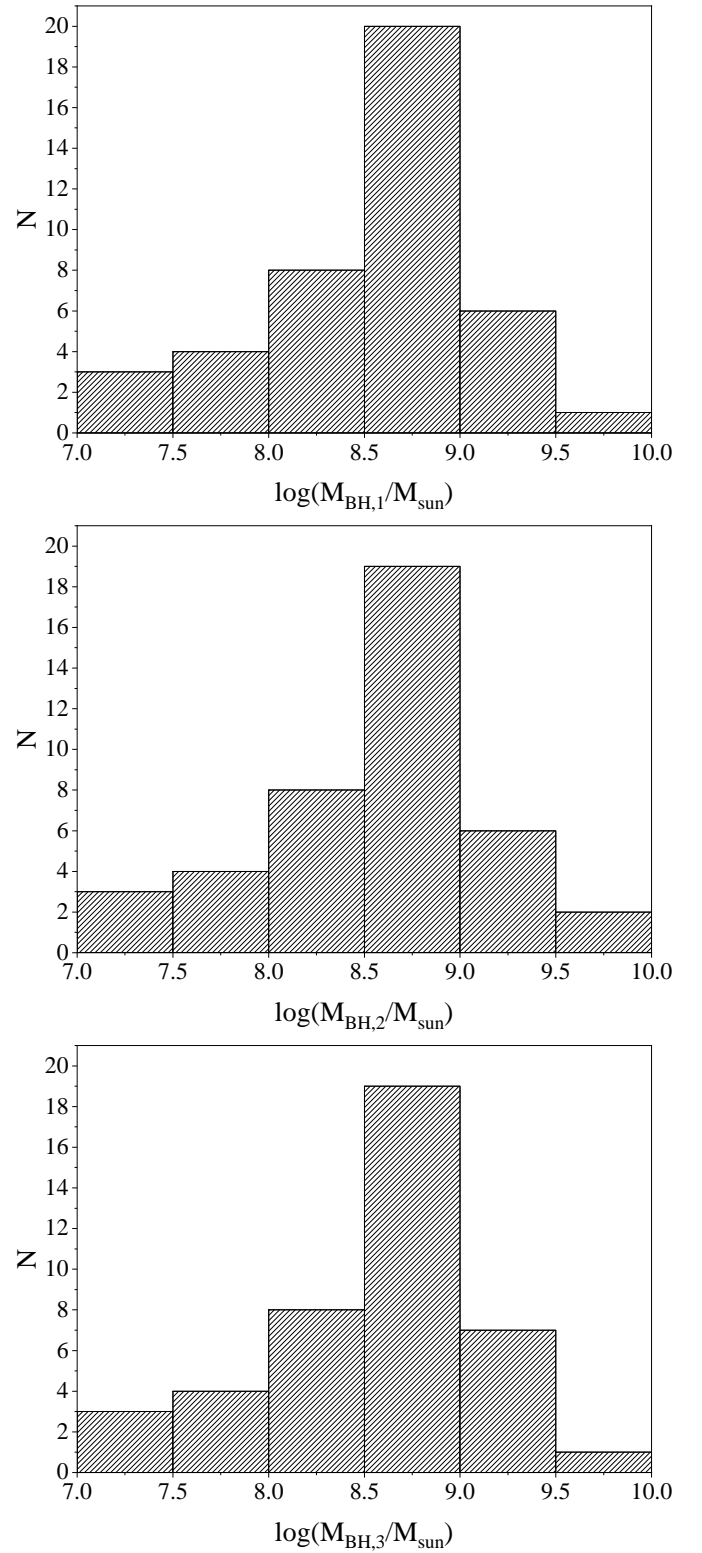


FIGURE 6 Distributions of estimated SMBH masses for 3 models.

(NLS1) a slope was ~ 1.25 (M. Piotrovich et al., 2023). The degree of the dependence of the spin on SMBH mass shows

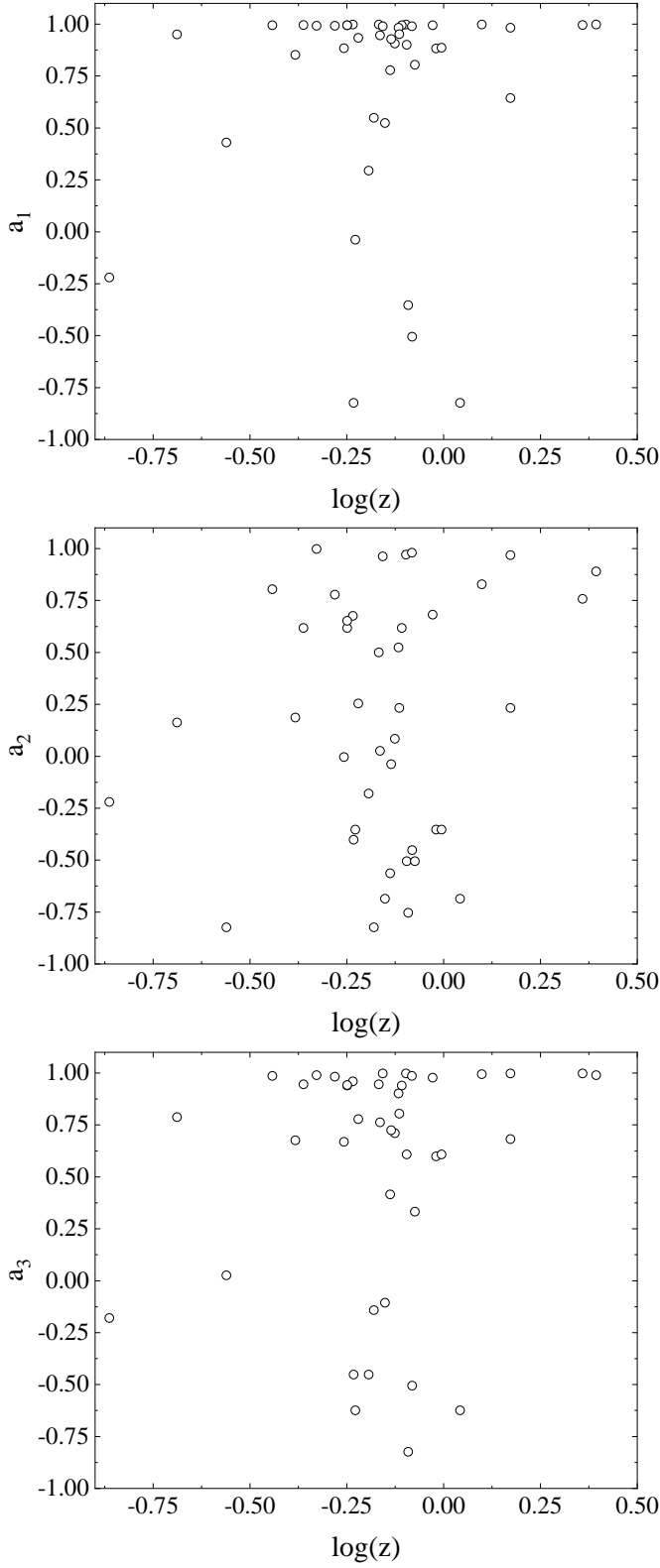


FIGURE 7 Dependencies of the spin on the redshift for 3 models.

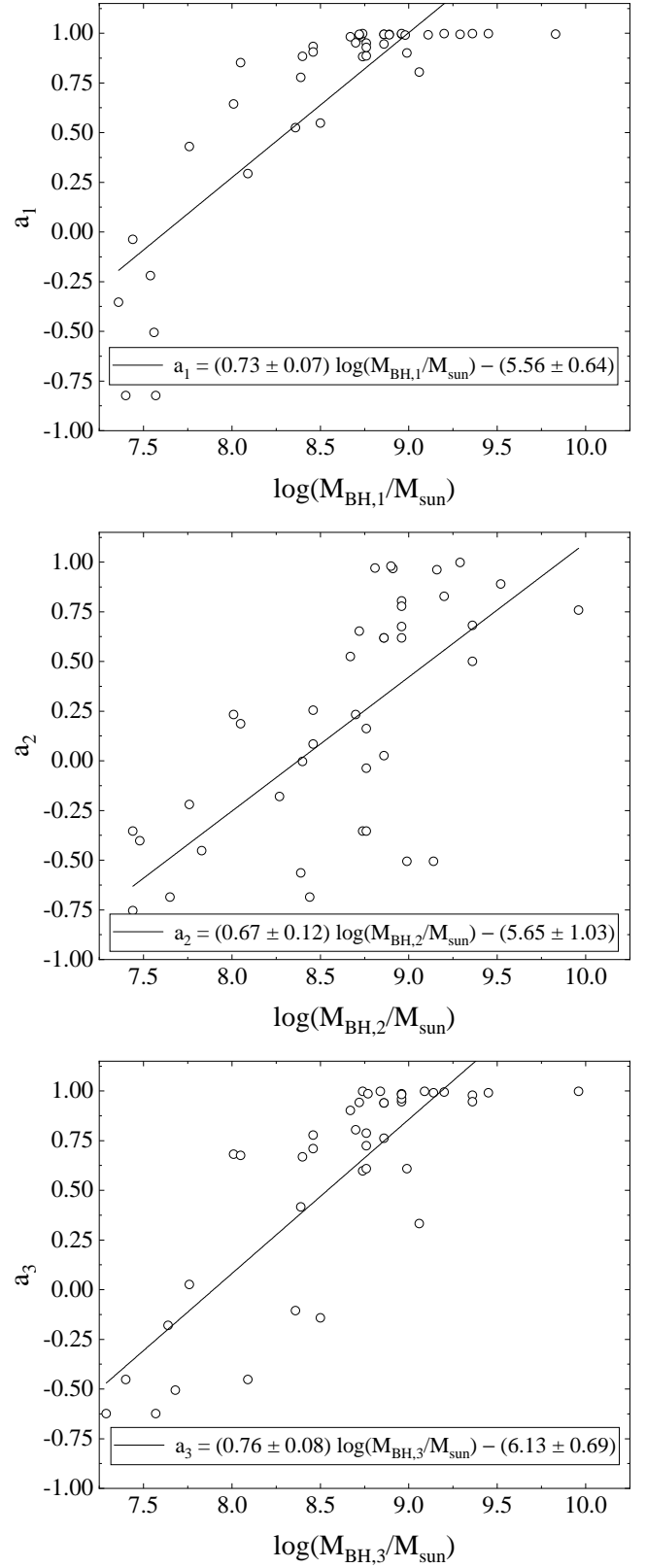


FIGURE 8 Dependencies of the spin on the SMBH mass for 3 models.

how quickly spin grows with increasing mass and, accordingly, speaks about the mechanism of mass growth. Rapid spin growth occurs due to the disk accretion, and slow growth occurs due to the chaotic accretion (for example, SMBH mergers), during which spin can even decrease. Thus, red quasars are in the middle between Seyferts and NLS1, which may indicate, for example, that the red quasars have both types of accretion and contain both Seyferts and NLS1 type objects.

Fig. 9 demonstrates dependencies of the spin value on the bolometric luminosity for 3 models. For first model there is moderate correlation between parameters (Spearman coef. is 0.51). For second model correlation is very weak (Spearman coef. is 0.13). And for third model correlation is weak-to-moderate (Spearman coef. is 0.35). Linear fitting gives us:

$$\begin{aligned} a_1 &= (0.46 \pm 0.09) \log(L_{\text{bol}}[\text{erg/s}]) - (20.87 \pm 4.14), \\ a_2 &= (0.20 \pm 0.13) \log(L_{\text{bol}}[\text{erg/s}]) - (9.24 \pm 6.00), \\ a_3 &= (0.43 \pm 0.11) \log(L_{\text{bol}}[\text{erg/s}]) - (19.43 \pm 4.94). \end{aligned} \quad (9)$$

Note that fittings of second and third models can only be considered as a manifestation of a general trend. Slope value for first model 0.46 ± 0.09 is close to similar value for NLS1 (M. Piotrovich et al., 2023) 0.54 ± 0.05 , from which it can be assumed that the population of red quasars may contain NLS1 type galaxies.

5 | CONCLUSIONS

We estimated values of spin, mass and inclination angle for sample of 42 red quasars using 3 models (Du et al., 2014; Raimundo et al., 2012; Trakhtenbrot, 2014) assuming that all objects have geometrically thin accretion disks.

Our estimations show that for 2 objects: F2MS J1113+1244 and F2MS J1434+0935 with highest Eddington ratios ($l_E = 2.29$ and $l_E = 3.35$ respectively) our approach doesn't seem to work very well, which may indicate that this two objects have geometrically thick disk (or that the mass of these objects is determined incorrectly).

For six objects (SDSS J0036-0113, S82X 0040+0058, S82X 0118+0018, S82X 0303-0115, FBQS J1227+3214, S82X 2328-0028) all 3 models produce a negative spin value, which may indicate the presence of "retrograde" rotation where the SMBH and its accretion disk rotate in opposite directions, which can be evidence of a recent merger. We were able to find in the literature some additional evidences of recent merger for object FBQS J1227+3214 (Glikman et al., 2024).

Statistical analysis of estimated spin values and it's comparison with similar data on Seyfert galaxies (type 1, 2 and intermediate types) and Narrow Line Seyfert galaxies (NLS1) shows that red quasar population may contain Seyfert and NLS1 type galaxies with both disk and chaotic accretion types.

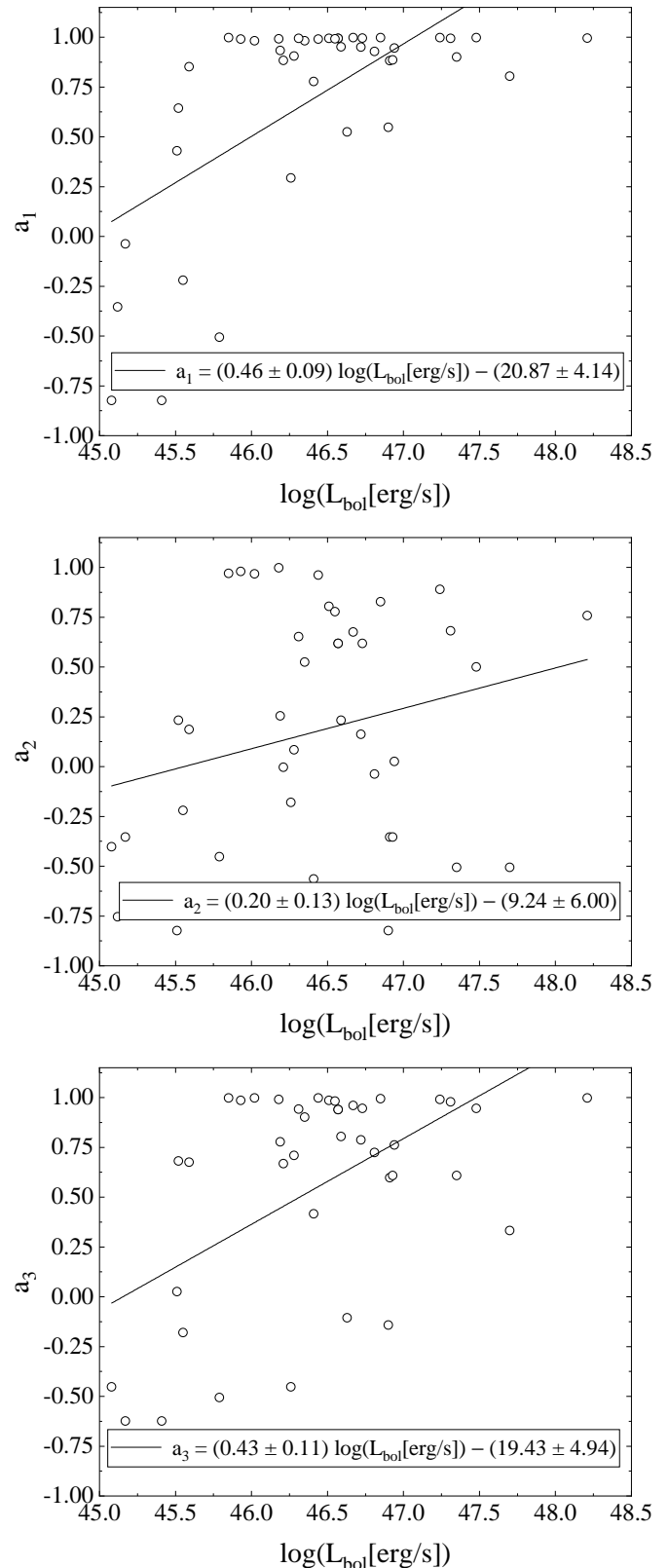


FIGURE 9 Dependencies of the spin on the bolometric luminosity for 3 models.

In general, we can say that of the three models used in this work the first model (Du et al., 2014) seems to be best suited for objects of this type.

ACKNOWLEDGMENTS

This research was supported by the state order of the Central Astronomical Observatory at Pulkovo, the planned research topic "MAGION" - Physics and evolution of stars and active galactic nuclei.

REFERENCES

- Afanasiev, V. L., Gnedin, Y. N., Piotrovich, M. Y., Natsvlshvili, T. M., & Buliga, S. D. (2018), *Astronomy Letters*, *44*, 362-369.
- Antonucci, R. (1993), *ARA&A*, *31*, 473-521.
- Bardeen, J. M., Press, W. H., & Teukolsky, S. A. (1972), *ApJ*, *178*, 347-370.
- Blandford, R. D., & Payne, D. G. (1982), *MNRAS*, *199*, 883-903.
- Blandford, R. D., & Znajek, R. L. (1977), *MNRAS*, *179*, 433-456.
- Collin, S., & Kawaguchi, T. (2004), *A&A*, *426*, 797-808.
- Daly, R. A. (2011), *MNRAS*, *414*, 1253-1262.
- Davis, S. W., & Laor, A. (2011), *ApJ*, *728*, 98.
- Decarli, R., Labita, M., Treves, A., & Falomo, R. (2008), *MNRAS*, *387*, 1237-1247.
- Du, P., Hu, C., Lu, K.-X. et al. (2014), *ApJ*, *782*, 45.
- Garofalo, D., Evans, D. A., & Sambruna, R. M. (2010), *MNRAS*, *406*, 975-986.
- Georgakakis, A., Clements, D. L., Bendo, G., Rowan-Robinson, M., Nandra, K., & Brotherton, M. S. (2009), *MNRAS*, *394*(1), 533-546.
- Glikman, E., LaMassa, S., Piconcelli, E., Urry, M., & Lacy, M. (2017), *ApJ*, *847*(2), 116.
- Glikman, E., LaMassa, S., Piconcelli, E., Zappacosta, L., & Lacy, M. (2024), *MNRAS*, *528*(1), 711-725.
- Glikman, E., Urrutia, T., Lacy, M. et al. (2012), *ApJ*, *757*(1), 51.
- Kim, D., & Im, M. (2018), *A&A*, *610*, A31.
- Kim, D., Im, M., Glikman, E., Woo, J.-H., & Urrutia, T. (2015), *ApJ*, *812*(1), 66.
- Krolik, J. H. (2007), Making black holes visible: accretion, radiation, and jets. In 2007 STScI Spring Symposium on Black Holes p. 309-321.
- Krolik, J. H., Hawley, J. F., & Hirose, S. (2007), The Relationship between Accretion Disks and Jets. In *Revista Mexicana de Astronomia y Astrofisica*, vol. 27 Vol. 27, p. 1-7.
- LaMassa, S. M., Glikman, E., Brusa, M. et al. (2017), *ApJ*, *847*(2), 100.
- LaMassa, S. M., Ricarte, A., Glikman, E. et al. (2016), *ApJ*, *820*(1), 70.
- Lawther, D., Vestergaard, M., Raimundo, S., & Grupe, D. (2017), *MNRAS*, *467*(4), 4674-4710.
- Lyke, B. W., Higley, A. N., McLane, J. N. et al. (2020), *ApJS*, *250*(1), 8.
- Novikov, I. D., & Thorne, K. S. (1973), Astrophysics of black holes. In C. Dewitt & B. S. Dewitt (Eds.), *Black Holes (Les Astres Occlus)* p. 343-450. New York: Gordon and Breach.
- Piotrovich, M., Buliga, S., & Natsvlshvili, T. (2023), *Universe*, *9*(4), 175.
- Piotrovich, M. Y., Buliga, S. D., & Natsvlshvili, T. M. (2022), *Astronomische Nachrichten*, *343*(5), e10020.
- Raimundo, S. I., Fabian, A. C., Vasudevan, R. V., Gandhi, P., & Wu, J. (2012), *MNRAS*, *419*, 2529-2544.
- Richards, G. T., Lacy, M., Storrie-Lombardi, L. J. et al. (2006), *ApJS*, *166*, 470-497.
- Shakura, N. I., & Sunyaev, R. A. (1973), *A&A*, *24*, 337-355.
- Thorne, K. S. (1974), *ApJ*, *191*, 507-520.
- Trakhtenbrot, B. (2014), *ApJ*, *789*, L9.
- Urrutia, T., Lacy, M., Spoon, H., Glikman, E., Petric, A., & Schulz, B. (2012), *ApJ*, *757*(2), 125.
- Urry, C. M., & Padovani, P. (1995), *PASP*, *107*, 803.

How cite this article: M.Yu. Piotrovich, S.D. Buliga, and T.M. Natsvlshvili (2024), Red quasars: estimation of SMBH spin, mass and accretion disk inclination angle, *Astronomische Nachrichten*, *2024;00:1–6*.

How cite this article: M.Yu. Piotrovich, S.D. Buliga, and T.M. Natsvlshvili (2024), Red quasars: estimation of SMBH spin, mass and accretion disk inclination angle, *Astronomische Nachrichten*, *2024;00:1–6*.